Out of rock: A new look at the morphological and geochemical preservation of microfossils from the 3.46 Gyr-old Strelley Pool Formation

Frédéric Delarue, Francois Robert, Sylvie Derenne, Romain Tartèse, Clément Jauvion, Sylvain Bernard, Sylvain Pont, Adriana Gonzalez-Cano, Rémi Duhamel, Kenichiro Sugitani

▶ **To cite this version:**

Frédéric Delarue, Francois Robert, Sylvie Derenne, Romain Tartèse, Clément Jauvion, et al.. Out of rock: A new look at the morphological and geochemical preservation of microfossils from the 3.46 Gyr-old Strelley Pool Formation. Precambrian Research, 2020, 10.1016/j.precamres.2019.105472 . hal-03021289

HAL Id: hal-03021289
https://hal.science/hal-03021289

Submitted on 24 Nov 2020

HAL is a multi-disciplinary open access archive for the deposit and dissemination of scientific research documents, whether they are published or not. The documents may come from teaching and research institutions in France or abroad, or from public or private research centers.

L'archive ouverte pluridisciplinaire **HAL**, est destinée au dépôt et à la diffusion de documents scientifiques de niveau recherche, publiés ou non, émanant des établissements d'enseignement et de recherche français ou étrangers, des laboratoires publics ou privés.

Precambrian Research 336 (2020) 105472

Contents lists available at ScienceDirect

Precambrian Research

journal homepage: www.elsevier.com/locate/precamres

Out of rock: A new look at the morphological and geochemical preservation of microfossils from the 3.46 Gyr-old Strelley Pool Formation

Frédéric Delarue[a,b,*], François Robert[a], Sylvie Derenne[b], Romain Tartèse[c], Clément Jauvion[a,d], Sylvain Bernard[a], Sylvain Pont[a], Adriana Gonzalez-Cano[a], Rémi Duhamel[a], Kenichiro Sugitani[e]

[a] Muséum National d'Histoire Naturelle, Sorbonne Université, UMR CNRS 7590, IRD, Institut de Minéralogie, de Physique des Matériaux et de Cosmochimie, IMPMC, 75005 Paris, France
[b] Sorbonne Université, UPMC, CNRS, EPHE, PSL, UMR 7619 METIS, 4 place Jussieu, F-75005 Paris, France
[c] School of Earth and Environmental Sciences, The University of Manchester, Manchester M13 9PL, United Kingdom
[d] Sorbonne Université, UPMC MNHN, CNRS, Centre de Recherche en Paléontologie, Paris, France
[e] Department of Earth and Environmental Sciences, Graduate School of Environmental Studies, Nagoya University, Nagoya, Japan

ARTICLE INFO

Keywords:
Archean
Early life
Microfossils
NanoSIMS
Phosphorus

ABSTRACT

The biogenicity of most of the putative Archean organic-walled microfossils discussed in the literature remains debated. Here, we report morphological and geochemical characterizations of an assemblage of microfossils isolated from the 3.46 Gyr-old Strelley Pool Formation (Western Australia), thereby providing a new set of data on the oldest authentic microfossils on Earth. Isolated microstructures/microfossils were studied by combining scanning electron microscopy imaging and elemental analyses, Raman spectroscopy and nanoscale secondary ion mass spectrometry (NanoSIMS). We identified four morphological types, namely filaments, films, spheroids and lenses. A minority of spheroids, films and lenses exhibits a continuous wall cell surface and high N concentrations and substantial P contents (as suggested by $^{31}P^-/^{12}C_2^-$ ionic ratios), i.e. exceptionally high morphological and geochemical preservation levels. In addition to the detection of P within microfossil walls, P was also found within micrometric patches in lenses exhibiting a fusiform shape. These patches may be remains of polyphosphate granules possibly formed during sporulation, suggesting, in turn, that cellular organization appeared as soon as 3.46 Gyr ago.

1. Introduction

The multiple occurrences of organic–walled microfossils in the Archean geological record suggest the widespread presence of life on Earth as early as ~3.5–3.4 Gyr ago (e.g. Awramik et al., 1983; Walsh and Lowe, 1985; Walsh, 1992; Wacey et al., 2011; Sugitani et al., 2015a,b; Oehler et al., 2017; Kremer and Kazmierczak, 2017; Alleon et al., 2018; Schopf et al., 2018). Many filaments, spheroids, films, and lenses have been described in numerous Archean metasedimentary rocks, including the emblematic 3.46 Gyr-old cherts of the Strelley Pool Formation (SPF – Western Australia). The carbonaceous nature of SPF microfossils, their morphological complexity, their organization into chains and clusters, their carbon isotope and molecular signatures, and the reported taphonomic degradation features support their biogenicity (Sugitani et al., 2010, 2013, 2015a, Wacey et al., 2011, 2012; Lepot et al., 2013; Alleon et al., 2018). Nonetheless, some doubts remain about the biogenicity of some of SPF microstructures since (i) mineral biomorphs and carbonaceous/sulfur filamentous and spheroidal biomorphs may form abiotically (Garcia-Ruiz et al., 2003; Cosmidis and Templeton, 2016; Rouillard et al., 2018), (ii) film-like microstructures may result from hydrocarbon migration and condensation/polymerization during diagenesis (Lepot et al., 2013; Sugitani et al., 2010), and (iii) some vesicular volcanic glasses could mimic lenticular microstructures, especially fusiform ones (Wacey et al., 2018).

To date, the dataset available on SPF microfossils remains quite scarce, each previous study having focused on only a few specimens. Complementary investigations including palynology and geochemical analyses are required to document the morphology and chemistry of a representative collection of SPF microfossils, offering the possibility to use these microfossils as references for evaluating the biogenicity of other Archean organic microstructures of putative biogenic origin. We have thus investigated the morphological and geochemical features of

* Corresponding author at: Muséum National d'Histoire Naturelle, Sorbonne Université, UMR CNRS 7590, IRD, Institut de Minéralogie, de Physique des Matériaux et de Cosmochimie, IMPMC, 75005 Paris, France.
E-mail address: frederic.delarue@upmc.fr (F. Delarue).

https://doi.org/10.1016/j.precamres.2019.105472
Received 14 March 2019; Received in revised form 5 August 2019; Accepted 20 September 2019
Available online 21 September 2019
0301-9268/ © 2019 The Authors. Published by Elsevier B.V. This is an open access article under the CC BY-NC-ND license (http://creativecommons.org/licenses/BY-NC-ND/4.0/).

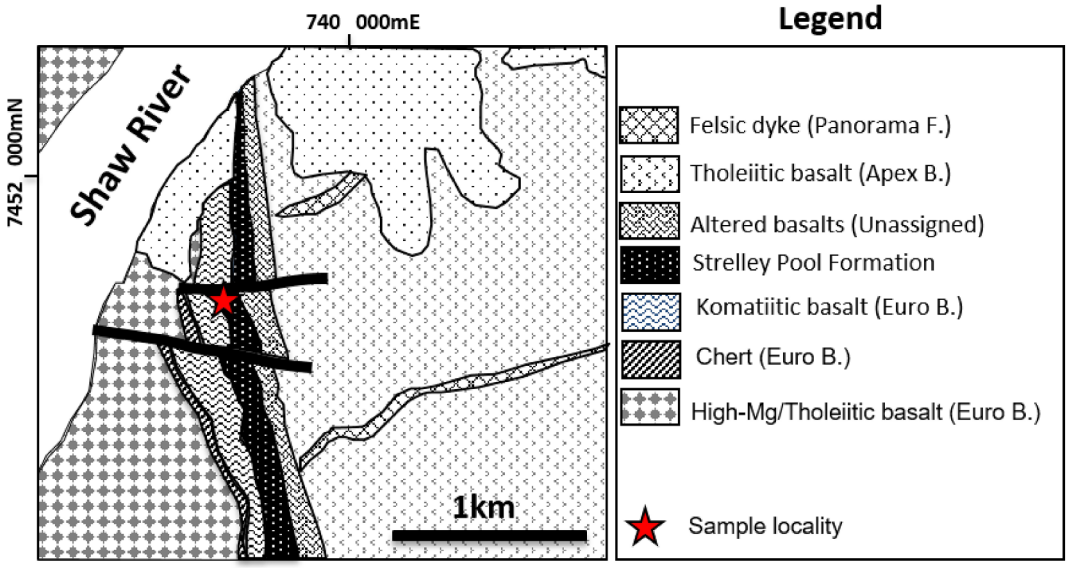

Fig. 1. Local geology around the Panorama greenstone belt (after Van Kranendonk, 1999; modified from Sugitani et al., 2013). Thick black lines correspond to faults.

an extensive set of SPF microfossils isolated from rock samples via acid maceration. Scanning electron microscopy (SEM) was used to document the morphological preservation of these isolated microfossils, while their geochemical characteristics were assessed using energy-dispersive X-ray spectroscopy (EDXS), Raman microspectroscopy and nanoscale secondary ion mass spectrometry (NanoSIMS), the latter allowing the estimation of nitrogen (N) and phosphorus (P) concentrations, thereby offering insights on the level of geochemical preservation of cell wall.

2. Material and methods

2.1. Geological background and studied sample

Numerous exposures of the SPF have been identified in the East Pilbara Terrane of the Pilbara Craton in Western Australia, and its depositional area is assumed to be at least 30,000 km^2 (Fig. 1; Hickman, 2008). This formation is typically 8–11 m thick and comprises various rock types, including siliciclastic sedimentary rocks such as sandstones and shales, carbonates (mainly bedded and stromatolitic dolomite), chert units, and volcanoclastic rocks, deposited mostly in shallow-water environments, and possibly in some terrestrial settings. Specifically, rocky coastal shoreline and beach environments, shallow-water marine carbonate platform, possible sabkha, tidal flat, and alluvial fans have been identified Allwood et al., 2006, 2007; Hickman, 2008; Sugitani et al., 2015a). In addition, units of the SPF have been affected by transient hydrothermal activity (Allwood et al., 2006, 2007, 2010; Hickman, 2008; Sugitani et al., 2010, 2013, 2018).

Carbonaceous cherts with abundant microfossils were selected for this study (Sugitani et al., 2013, 2015a). The sedimentary unit belonging to the SPF at this locality comprises a varicolored (black to pale green to gray) chert unit, a white chert breccia, and cross-laminated to thinly bedded pale-to-reddish-brown layers. Abundant microfossils were identified in the black chert that displays microscopically identifiable parallel laminations. It has been suggested that this black chert was deposited in a shallow (intertidal to sub-tidal) marine environment susceptible to hydrothermal inputs, as suggested by rare-earth element signatures and high concentrations of heavy metals (Allwood et al., 2007, 2010; Sugitani et al., 2013, 2018).

2.2. Isolation of carbonaceous microstructures/microfossils

Organic-walled microfossils were isolated from the SPF carbonaceous black chert using a modified version of the classical acid maceration procedure (Durand, 1980). A 'soft' acid maceration procedure was applied in order to minimize both potential physical and chemical degradations of organic microstructures. Prior to acid maceration, about 30 g of rock samples were fragmented into ~3 g rock chips rather than crushed into much finer grains. Rock chips were cleaned using bi-distilled water and a mixture of dichloromethane/ethanol (v/v: 2/1). Rock chips were then directly placed in a Teflon vessel filled with a mixture of HF/HCl (v/v: 9/1) at room temperature. After 48 h, successive centrifugation and rinsing steps using bi-distilled water were performed until reaching neutrality. The residual material was suspended in ethanol and filtered on polycarbonate filters (pore Ø = 10 µm). After ethanol evaporation, polycarbonate filters were fixed on carbon tape and coated with 20 nm of gold to prevent further contamination by atmospheric deposits.

2.3. SEM-EDXS and Raman microspectroscopy

SEM-EDXS imaging and analysis were performed on gold-coated filters using a TESCAN VEGA II at the French National Museum of Natural History (MNHN) with an accelerating voltage of 15 kV.

Raman microspectroscopy was carried out using a Renishaw InVIA microspectrometer equipped with a 532 nm green laser. The laser was focused on the sample by using a DMLM Leica microscope with a 50× objective. The spectrometer was first calibrated with a silicon standard before the analytical session. For each target, we determined the Raman shift intensity in the 1000 to 2000 cm^{-1} spectral window that includes the first-order defect (D) and graphite (G) peaks. A laser power below 1 mW was used to prevent any thermal alteration during the spectra acquisition. Spectra acquisition was achieved after two iterations using a time exposure of 40 s. Maximum heights in the 1250–1400 cm^{-1} and 1580–1625 cm^{-1} Raman shift range (D and G bands, respectively) were then measured and the intensity ratio between the D and G bands (I_D/I_G) was calculated. The Full Width at Half Maximum of the D1 band (FWHM-D1) was determined after Raman spectra decomposition into a combination of five Lorentzian/Gaussian bands (namely, D1, D2, D3, D4, and G).

In order to probe the carbon structural order of microstructures/microfossils, Raman microspectroscopy was performed after their identification through SEM-EDXS imaging, on gold-coated samples. Their average I_D/I_G ratio of 0.90 ± 0.13 is lower than the I_D/I_G ratio of 1.15 ± 0.02 obtained on randomly selected non goal-coated carbonaceous matter (n = 3). This discrepancy suggests that gold coating

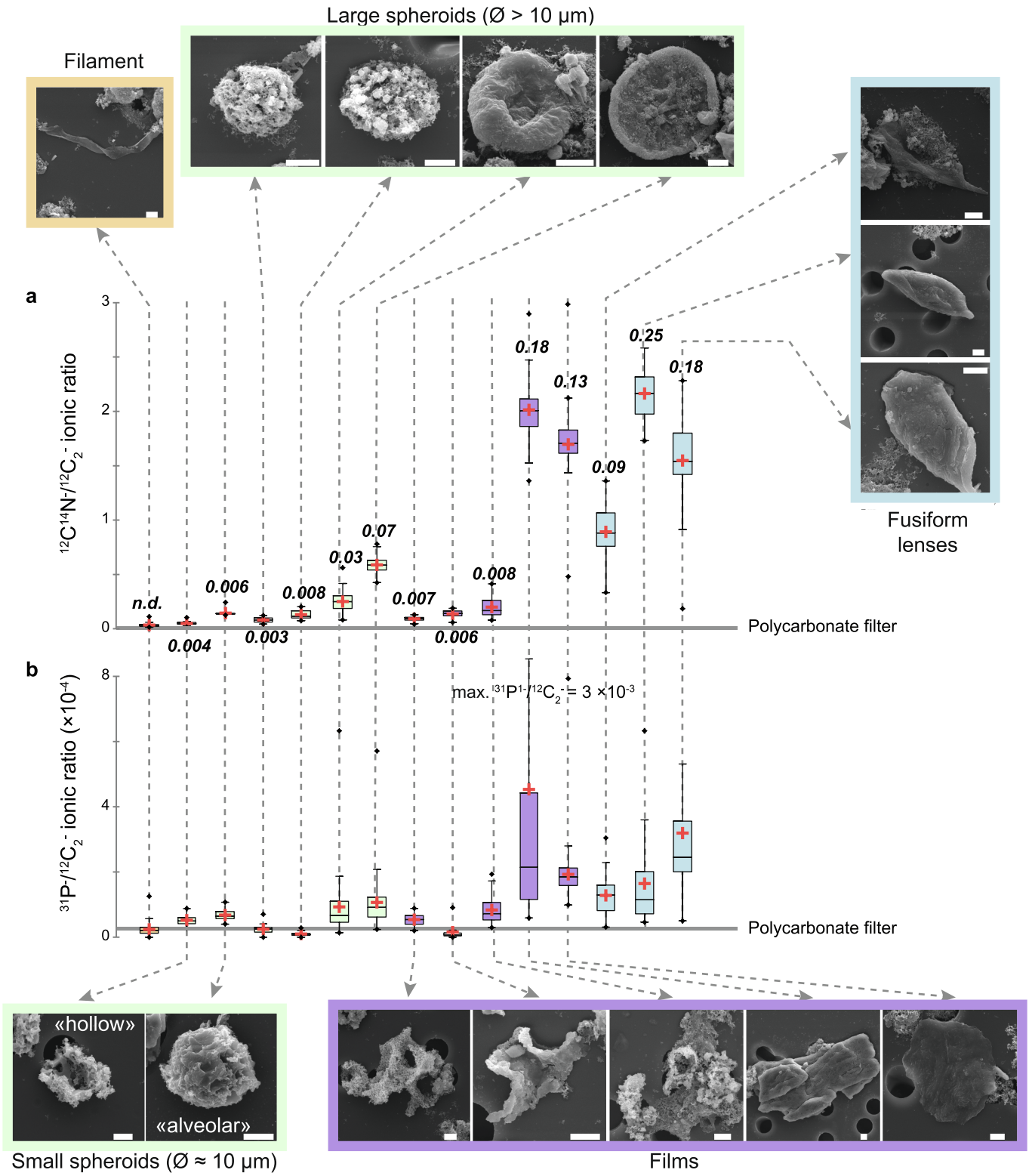

Fig. 2. NanoSIMS-derived quantitative $^{12}C^{14}N^-/^{12}C_2^-$ (a) and $^{31}P^-/^{12}C_2^-$ (b) ionic ratios determined on isolated organic-wall microfossils and/or microstructures. Light orange, green, purple and blue colors correspond to filament, spheroids, films and fusiform lenses, respectively. Numbers in bold italic indicate the bulk N/C ratio at the scale of individual microstructures/microfossils. "n.d." indicates a N/C atomic ratio too low to be computed. The horizontal grey lines correspond to the $^{12}C^{14}N^-/^{12}C_2^-$ and $^{31}P^-/^{12}C_2^-$ ionic ratios determined on the N- and P-free polycarbonate filter. White scale bars in all SEM images represent 5 µm. (For interpretation of the references to color in this figure legend, the reader is referred to the web version of this article.)

introduces a slight underestimation of the I_D/I_G ratio. In addition, we determined an average FWHM-D1 of about 96.0 ± 1.5 cm^{-1} on randomly selected non gold-coated carbonaceous matter. On gold-coated samples, an average FWHM-D1 of 106.5 ± 16.2 was determined suggesting that gold coating caused a slight overestimation of this parameter. Finally, Raman microspectroscopy was also performed on the polycarbonate filter to avoid any possible interference (Supplementary Fig. 1).

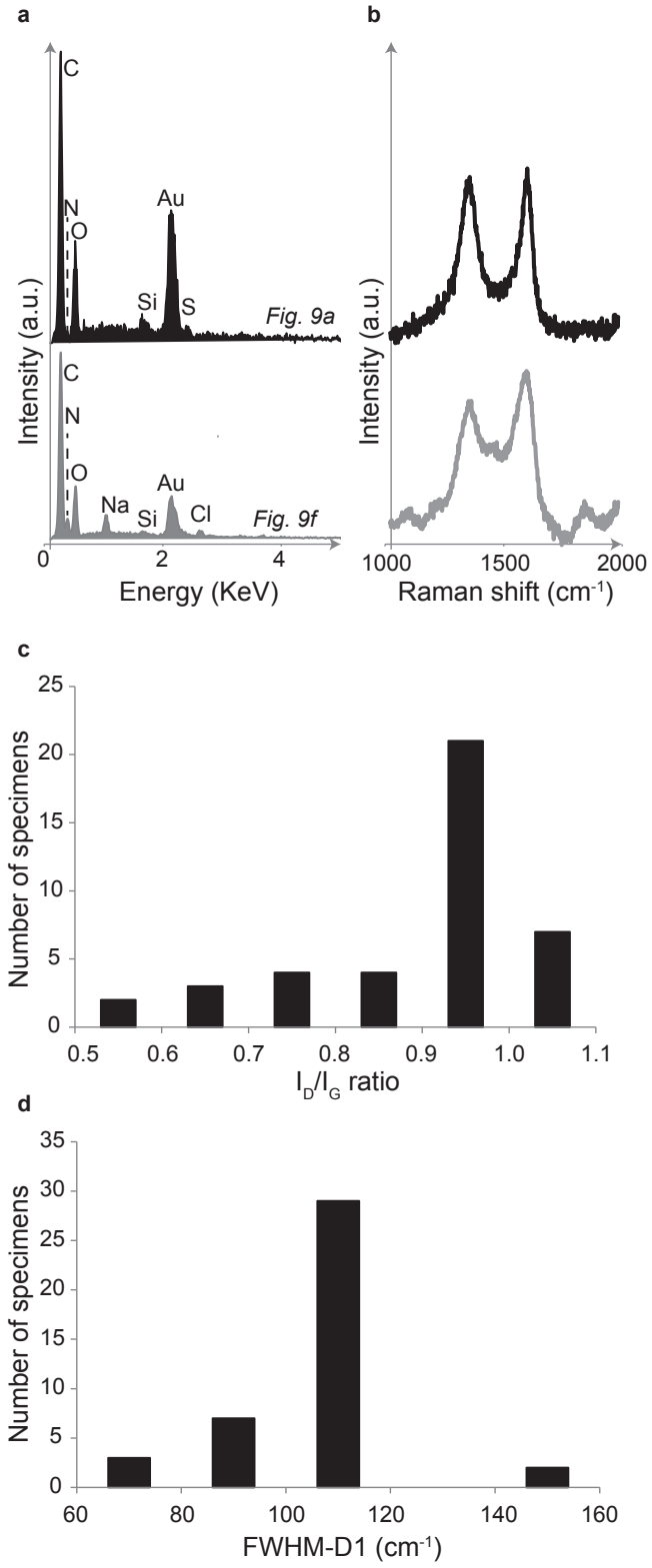

Fig. 3. (a) SEM-EDXS and (b) Raman spectra acquired on specimens presented in Fig. 9a and 9f. (c) Distribution of I_D/I_G ratios and of (d) FWHM-D1 values determined on isolated microstructures and on randomly selected carbonaceous particles (n = 41).

2.4. Nanoscale secondary ion mass spectrometry

Standards and isolated carbonaceous microstructures were analyzed using a CAMECA NanoSIMS 50 using a Cs^+ primary ion beam. Before measurements, pre-sputtering was performed over 30 × 30 μm^2 areas using a 700 pA primary current (750 µm aperture diaphragm) to avoid surficial contamination, and achieve Cs^+ saturation fluence and constant secondary ion count rates (Thomen et al., 2014). Analyses were then carried out using a 1.4–80 pA primary current (200 µm aperture diaphragm) on smaller areas to avoid pre-sputtering edge artifacts. The secondary molecular species $^{12}C_2^-$, $^{12}C^{14}N^-$ and $^{31}P^-$ were collected simultaneously in electron multipliers for 10–15 min.

The NanoSIMS raw data were corrected for a 44 ns dead time on each electron multiplier and processed using the Limage software (developed by L. Nittler, Carnegie Institution, Washington DC, USA). Regions of interest (ROI) were drawn as a grid on standards and microfossils/microstructures. The external reproducibility of measured $^{12}C^{14}N^-/^{12}C_2^-$ and $^{31}P^-/^{12}C_2^-$ ratios was determined through multiple measurements on a homogeneous and flat resin standard and on a type III kerogen (Supplementary Table 1; Thomen et al., 2014; Delarue et al., 2017). The $^{12}C^{14}N^-/^{12}C_2^-$ and $^{31}P^-/^{12}C_2^-$ ratios determined for each square of a grid were used to calculate median and mean $^{12}C^{14}N^-/^{12}C_2^-$ and $^{31}P^-/^{12}C_2^-$ ratios for standards and carbonaceous microfossils/microstructures. In contrast to mean values, the use of median values mitigates the potential effect of extreme values that could be related to microtopographic effects or ion emission hotspots occurring during sputtering of 3D object such as isolated microstructures. The external reproducibility on the median and mean values of the $^{12}C^{14}N^-/^{12}C_2^-$ molecular ionic ratio was about 8 and 7%, respectively, on the type III kerogen, and about 12 and 11%, respectively, on the resin (Supplementary Table 1). Since the resin standard is P-free, only the type III kerogen was used to compute the external reproducibility on the $^{31}P^-/^{12}C_2^-$ ratio, yielding 19 and 16% reproducibility on the $^{31}P^-/^{12}C_2^-$ median and mean values, respectively (Supplementary Table 1).

At the scale of individual microfossils, N/C atomic ratios were determined according to the procedure defined in Delarue et al. (2017,2018c). In both standards and microfossils/microstructures, correlations between the $^{12}C_2^-$ and $^{12}C^{14}N^-$ ion emissions determined in each ROI were tested using Spearman's rank correlation. In the presence of a significant spatial relationship between the $^{12}C_2^-$ and $^{12}C^{14}N^-$ ion emissions, linear regressions were performed to calculate the value of the slope (α) and its associated standard error ($1\sigma_{reg}$) following:

$$1\sigma_{reg} = \sqrt{\sum (yi - \hat{y}i)^2/(n-2)} / \sqrt{\sum (xi - \bar{x})^2} \quad (1)$$

where yi is the emission of the $^{12}C^{14}N^-$ ion measured by NanoSIMS, ŷi is the emission of the $^{12}C^{14}N^-$ ion determined by linear regression, xi is the emission of the $^{12}C_2^-$ ion measured by NanoSIMS, $\bar{X}$ the average value of the emissions of the $^{12}C_2^-$ ion and where n is the number of ROIs. The relationship between the slopes determined on type III kerogen and resin standards and their respective bulk N/C atomic ratios (Supplementary Table 1) was used to calibrate the determination of N/C atomic ratio on individual carbonaceous microfossils/ microstructures (Supplementary Fig. 1), which was associated with a standard error ($1\sigma_{rep}$) of about 7%. The final uncertainty ($1\sigma_{tot}$) associated with the calculated N/C atomic ratios was determined as follow:

$$1\sigma_{tot} = \sqrt{1\sigma_{reg}^2 + 1\sigma_{rep}^2} \quad (2)$$

3. Results and discussion

3.1. Syngenecity of isolated carbonaceous microstructures

Four morphological types (filaments, films, spheroids and lenses) have been recognized in the acid maceration residue (Fig. 2). SEM-EDXS analyses reveal that all studied microstructures/microfossils were almost exclusively composed of OM (C, N, S and O; Fig. 3a), and as such, are not carbon-coated mineral biomorphs. These carbonaceous

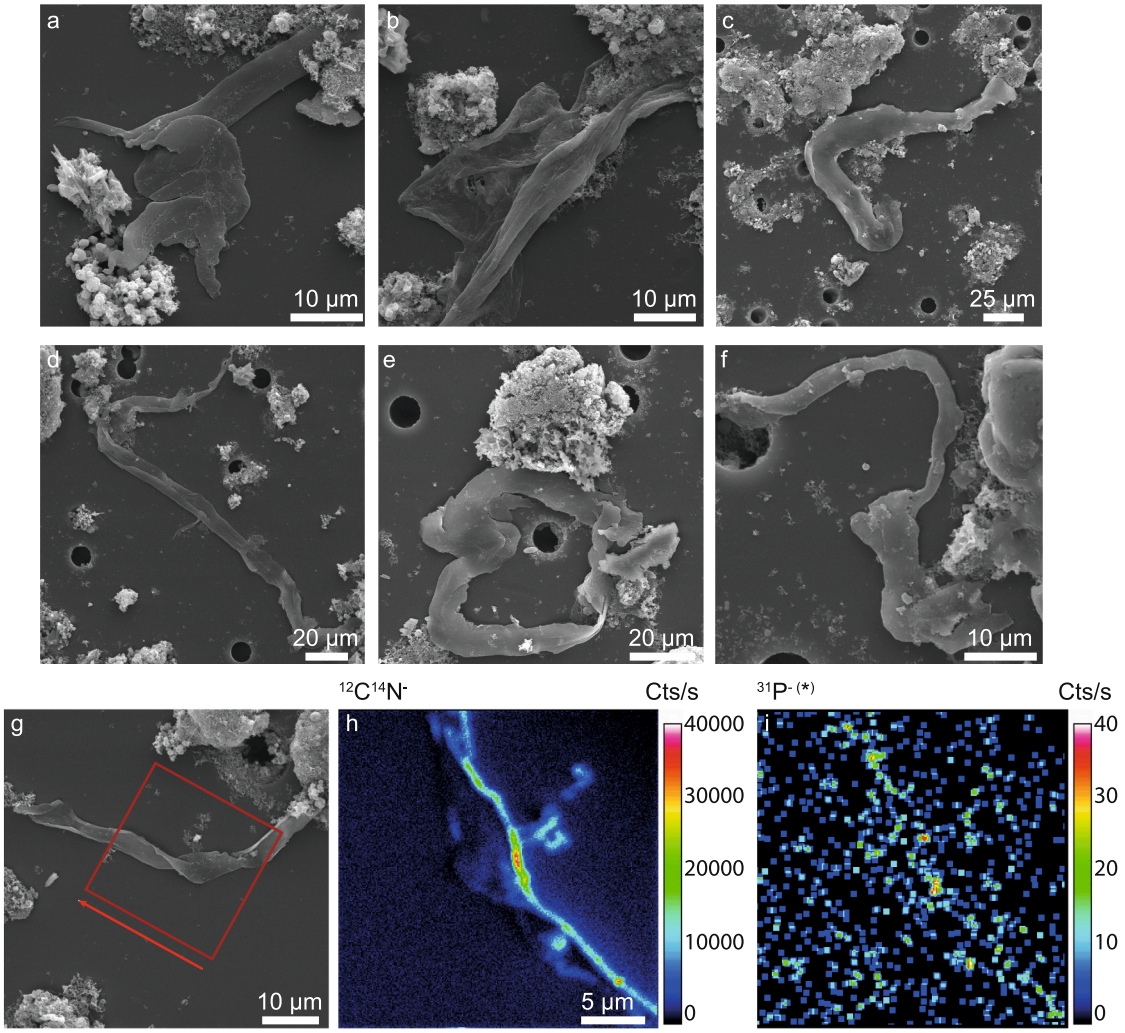

Fig. 4. (a-f) SEM images of isolated filaments. (g) SEM image and corresponding (h, i) NanoSIMS ion images ($^{12}C^{14}N^-$ and $^{31}P^-$, respectively) of an isolated filament. The color scale shows the secondary ion emission intensities per pixel. The asterisk indicates that the $^{31}P^-$ ion image corresponds to a "smoothed image", in which $^{31}P^-$ intensities are averaged over regions of 3 × 3 pixels.

microstructures display Raman spectra exhibiting a first-order region (1100–1800 cm^{-1}) with two broad bands at *ca.* 1350 (D band) and 1600 cm^{-1} (G band) resulting from the presence of disorder (in-plane defects and heteroatoms) and from C=C stretching vibration in poly-aromatic layers (Jehlicka and Beny, 1992), respectively (Fig. 3b). The unimodal distributions of the I_D/I_G ratios and of the FWHM-D1 values determined in identified microstructures and in randomly selected particles points to the existence of a single population of carbon structural order within the SPF (Fig. 3c-d). Hence, more than half of the microfossils investigated exhibit I_D/I_G and FWHM-D1 values of ca. 0.95 and 110, respectively (Fig. 3). When taking into account the effect of gold-coating, these I_D/I_G and FWHM-D1 values obtained here on SPF microfossils are typical for OM having experienced carbonization (Delarue et al., 2016), corresponding to prehnite-pumpellyite to lower greenschist metamorphism (Delarue et al., 2016). In addition, I_D/I_G and FWHM-D1 values determined on syngenetic OM from the SPF exhibit values of ca. 1 and 100, respectively (Allwood et al., 2006; Sugitani et al., 2010; Wacey et al., 2011; Lepot et al., 2013; Delarue et al., 2016) close to the ones determined in this study. These values are therefore consistent with the thermal history of the SPF, supporting in turn, the syngenecity of the studied microfossils.

3.2. Filaments from the Strelley Pool Formation

Filaments are observed in a wide range of Archean rocks (Awramik et al 1983; Walsh and Lowe, 1985; Rasmussen, 2000; Ueno et al., 2001; Westall et al., 2001; Kiyokawa et al., 2006; Sugitani et al., 2007, 2010; Schopf et al., 2018), and constitute the carbonaceous microstructures for which biogenicity remains a priori the most disputable (Buick, 1984, Sugitani et al., 2010). Filamentous microstructures from the SPF include both thin (< 5µm) non tubular thread and thin to relatively broad (*ca.* 20 µm) hollow tubes (Sugitani et al., 2010, 2013). The presently observed filaments display a 2D flat and smooth surface morphology (Fig. 4). In addition, no difference in the $^{12}C^{14}N^-/^{12}C_2^-$ and $^{31}P^-/^{12}C_2^-$ ionic ratios could be observed between the filament specimen analyzed here and the N- and P-free polycarbonate filter (Fig. 2), suggesting a virtual lack of N and P in the SPF filaments. Such an observation can be extended to all microfossils for which the $^{12}C^{14}N^-/^{12}C_2^-$ and $^{31}P^-/^{12}C_2^-$ ionic ratios cannot be distinguished from those determined on the polycarbonate filter in NanoSIMS images. Combination of palynology and of microscale analyses therefore does not provide new additional insights about the biogenicity of filament microstructures.

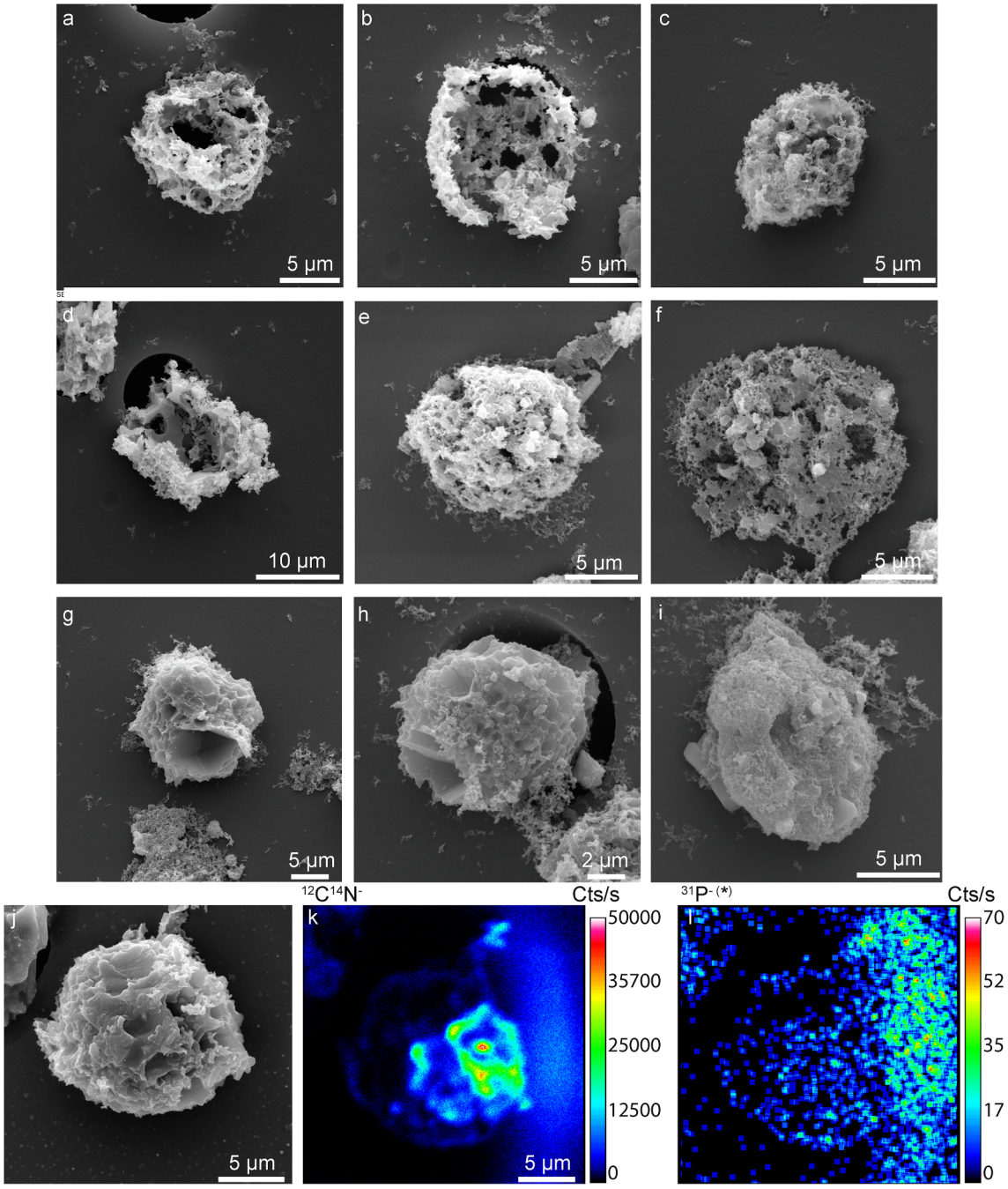

Fig. 5. (a-i) SEM images of small "hollow" and "alveolar" spheroids. (j) SEM images of an "alveolar" spheroid microfossil, and (k,l) corresponding NanoSIMS ion images of $^{12}C^{14}N^-$ and $^{31}P^-$, respectively. The asterisk indicates that the $^{31}P^-$ ion image corresponds to a "smoothed image", in which $^{31}P^-$ intensities are averaged over regions of 3 × 3 pixels.

3.3. The spheroid morphological type hides a large 3.46 Gyr-old biodiversity

A diverse population of spheroidal microstructures showing large variation in diameter size can be recognized in the acid maceration residue, including small spheroids (Ø ≈ 10 µm), carbonaceous globules (Ø < 1 µm) and large spheroids (Ø > 10 µm) (Fig. 5). Most spheroids are around 10 µm in diameter, consistent with previous observations on petrographic thin sections (Sugitani et al., 2010, 2013). Among them have been observed hollow specimens likely corresponding to cell lumina (Sugitani et al., 2010; Wacey et al., 2012) and displaying wrinkled and broken outer surfaces, suggesting brittle deformation during fossilization (Fig. 5a, b and d). It has been proposed that their discontinuous surface formed through post-mortem displacement of OM during siliceous or pyrite crystal growth (Wacey et al., 2012; Lepot et al., 2013). The hollow spheroids observed here show that, despite their discontinuous surfaces, they still present a coherent 3D morphology and have resisted the acid maceration procedure.

"Alveolar" carbonaceous spheroids, which have never been reported in Archean rocks so far, are also observed in the SPF acid-maceration residue (Ø ≈ 10 µm diameter; Fig. 2; Fig. 5g, h and j). They exhibit a continuous surface characterized by the occurrence of polygonal alveoli corresponding to submicron-size imprints of quartz crystal growth, highlighting the plasticity of these spheroids. These spheroids likely originate from precursors distinct from those of the hollow and brittle spheroids described above. In fact, their distinctive taphonomic features may point to distinct original properties.

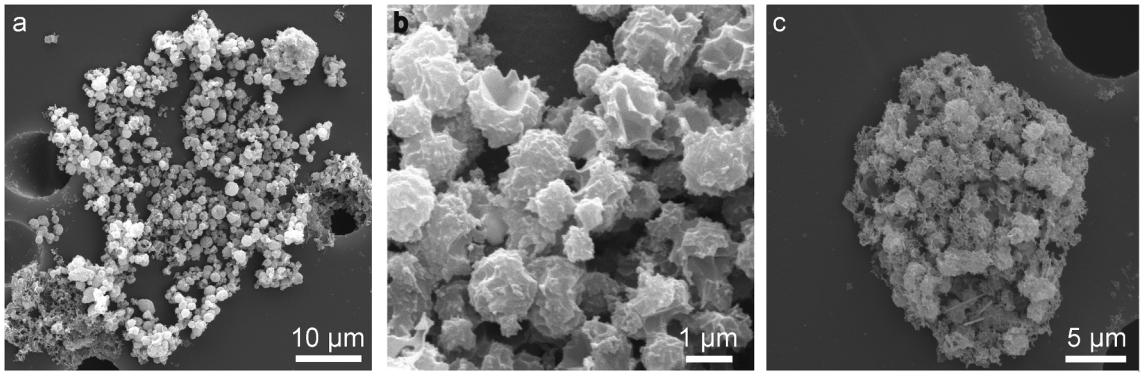

Fig. 6. (a) Aggregation of micrometric carbonaceous globules. (b) Zoom on micrometric carbonaceous globules, showing a maximum size of around 1 µm. (c) Carbonaceous globules possibly related to the degradation of a pseudo spheroid.

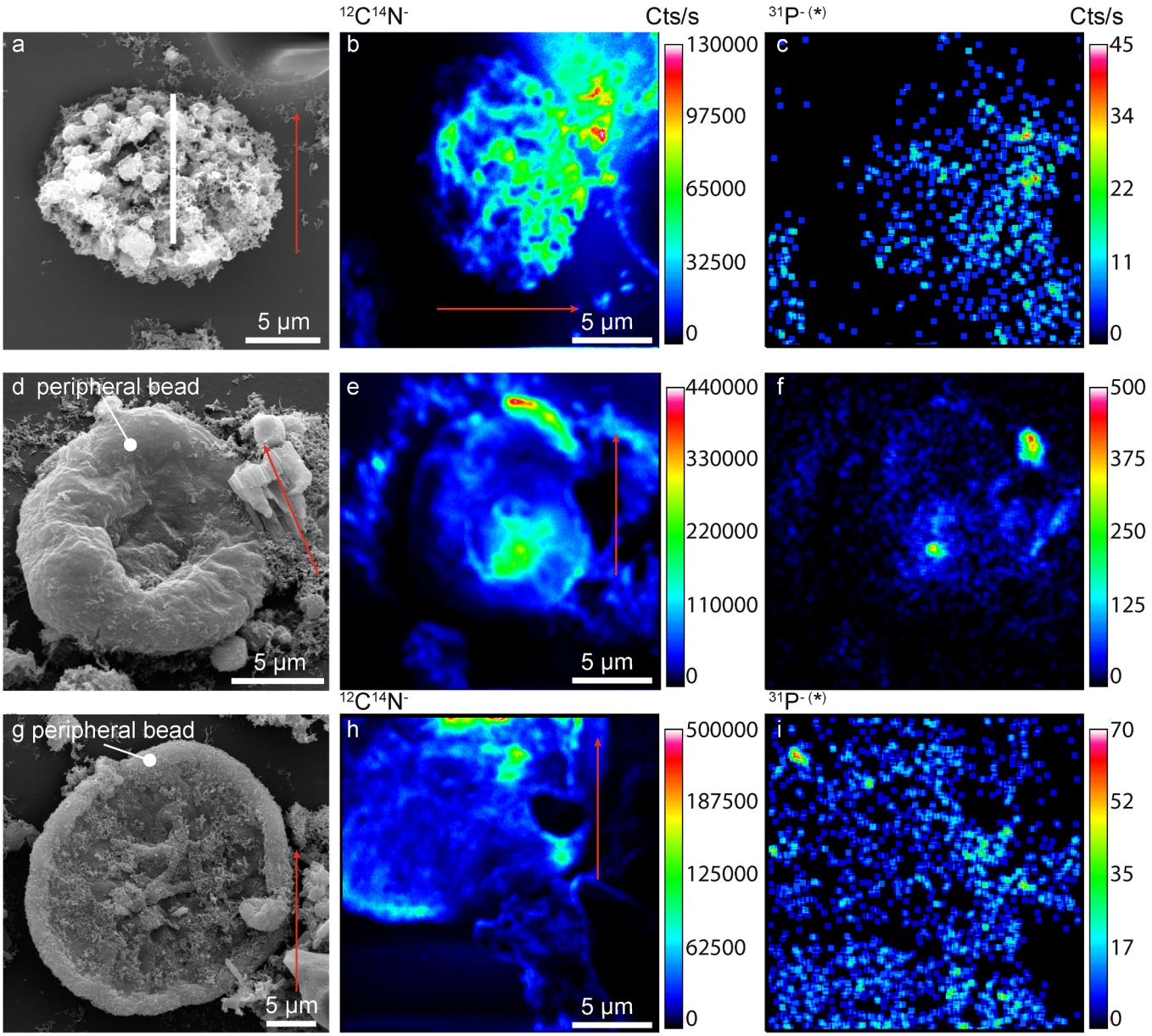

Fig. 7. (a, d, g) SEM images of isolated large spheroids and (b, c, e , f, h, i) corresponding NanoSIMS ion images of $^{12}C^{14}N^-$ and $^{31}P^-$. The asterisk indicates that the $^{31}P^-$ ion image corresponds to a "smoothed image", in which $^{31}P^-$ intensities are averaged over regions of 3 × 3 pixels.

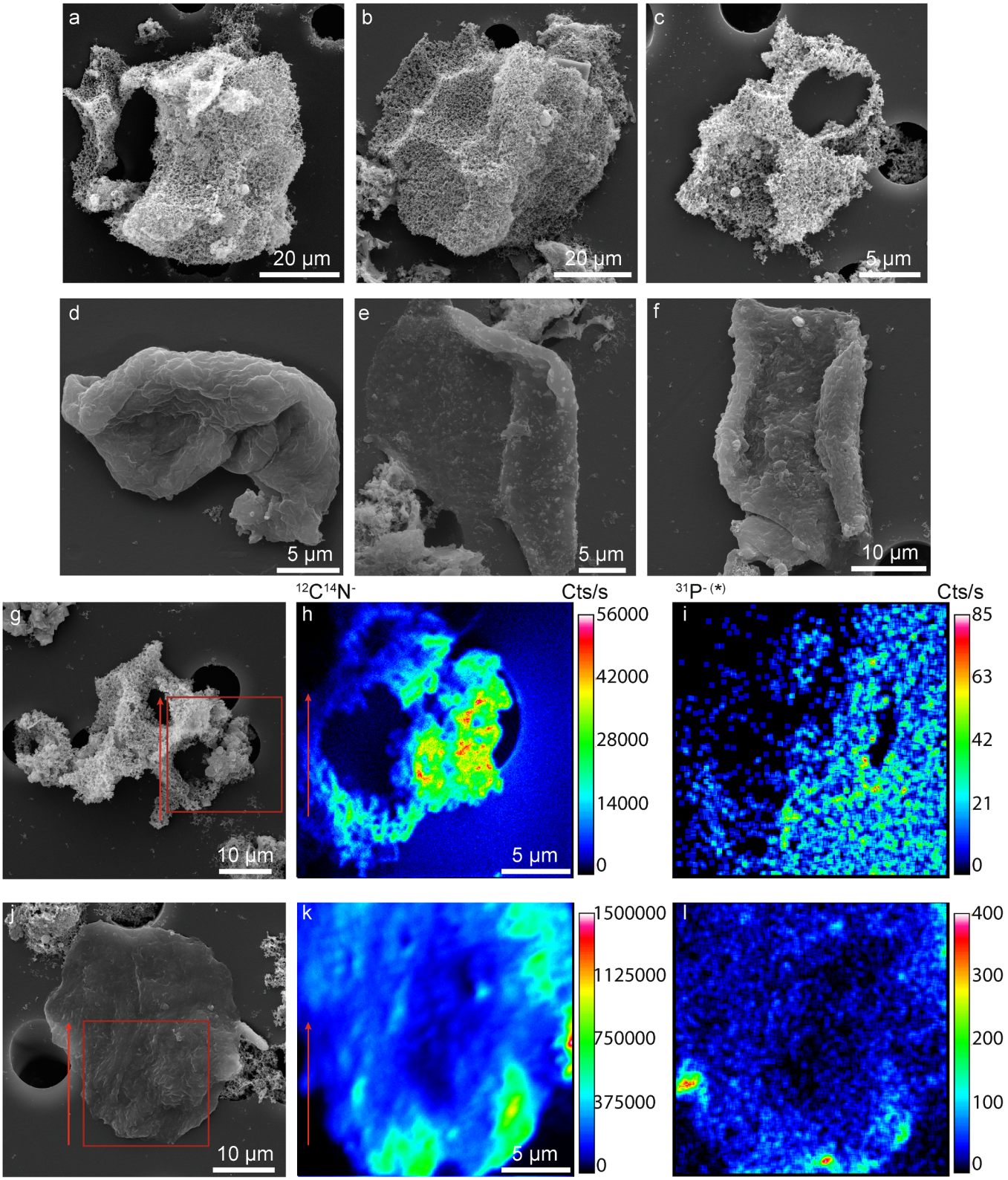

Fig. 8. (a-g,j) SEM images of isolated films, and (h,i,k,l) corresponding NanoSIMS ion images of $^{12}C^{14}N^-$ and $^{31}P^-$. The asterisk indicates that the $^{31}P^-$ ion image corresponds to a "smoothed image", in which $^{31}P^-$ intensities are averaged over regions of 3 × 3 pixels.

In addition to spheroids, micron-sized carbonaceous globules were also observed (Fig. 6). It has been suggested that such micron-sized carbonaceous globules represent remains of oil droplets (Buick, 1990; Lepot et al., 2013). A previous NanoSIMS investigation on Archean microfossils -carried out *in situ* in thin sections- showed that these carbonaceous globules can be contiguous and aligned, as remnants of cell walls. (Oehler et al., 2009). Similarly, some carbonaceous globules observed in the SPF acid-maceration residue were shown to aggregate into a large pseudo-spheroid (Fig. 6c). This is consistent with the idea that carbonaceous globules originated from oil droplets that would

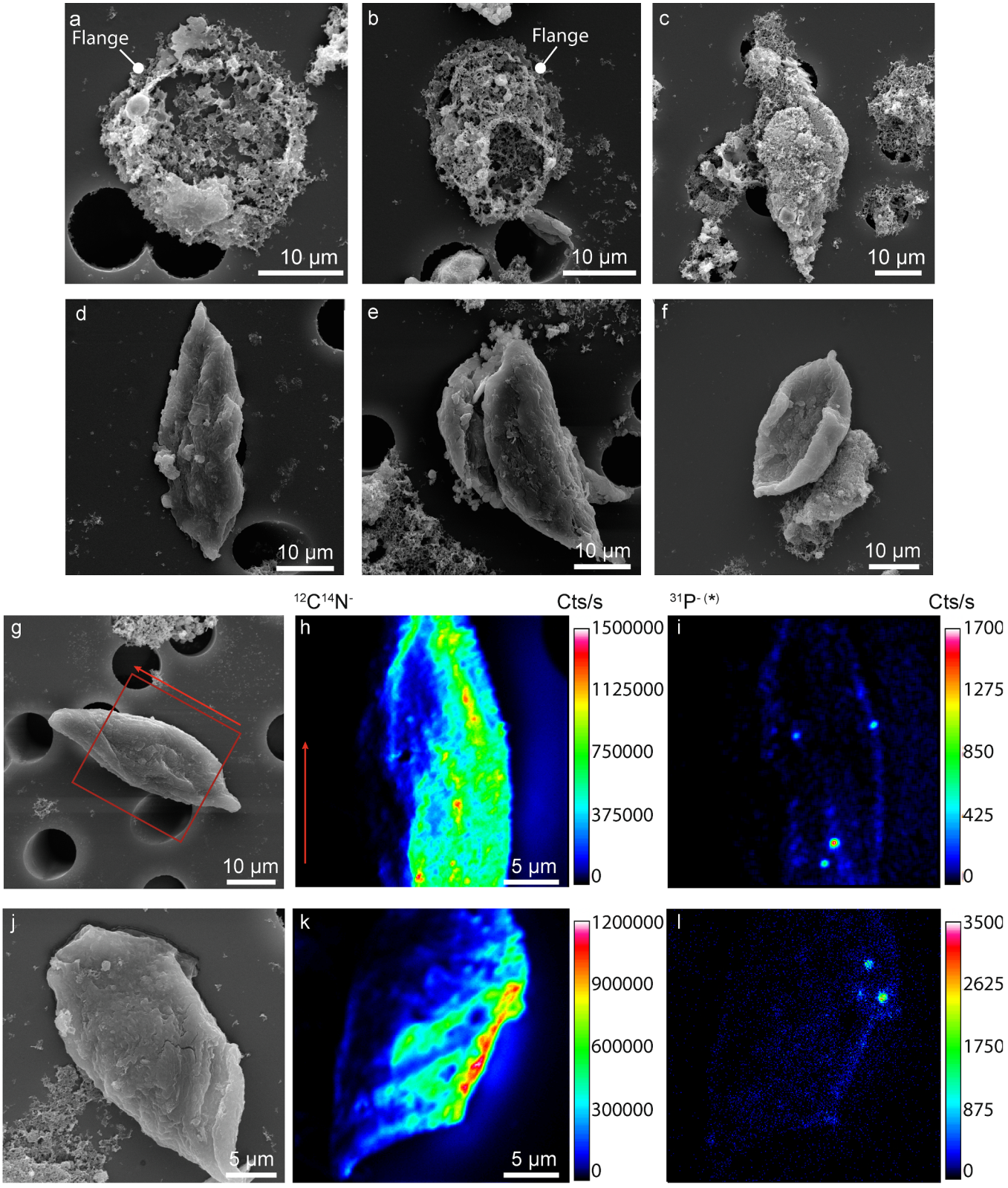

Fig. 9. (a-c) SEM images of isolated flanged lenses. (d-f) SEM images of non-flanged fusiform carbonaceous microstructures. (g, j) SEM images of non-flanged fusiform carbonaceous microstructures, and (h, i, k, l) corresponding NanoSIMS ion images of $^{12}C^{14}N^-$ and $^{31}P^-$. The asterisk indicates that the $^{31}P^-$ ion image corresponds to a "smoothed image", in which $^{31}P^-$ intensities are averaged over regions of 3 × 3 pixels.

have been expelled from microfossils and would have then solidified (Lepot et al., 2013). If correct, such carbonaceous globules should be seen as pyrobitumen (also called solid bitumen), i. e. insoluble OM formed during the solidification of generated bitumen (Curiale, 1986, Bernard and Horsfield, 2014; Sanei et al., 2015). As early silicification of Archean sediments may have drastically reduced rock porosity (Ledevin et al., 2014), bitumen migration during thermal alteration may have been hindered, favoring its solidification close to its

generating source, i.e. the carbonaceous microstructure/microfossil. This supports recent findings that Archean silicified metasediments can act as a source-reservoir system containing a mixture of kerogen (insoluble OM from which bitumen and pyrobitumen originate), pyrobitumen and bitumen (Delarue et al., 2018a).

Some large spheroids, with a diameter higher than 15 µm, present reticulated or fuzzy surfaces (Fig. 2; Fig. 7a) and are characterized by low N/C atomic ratios of *ca.* 10^{-2}-10^{-3} (Fig. 2). Although rare, other large spheroids are characterized by a continuous surface and by a peripheral bead giving them a spheroidal dish-like morphology (Fig. 7d, g). These large spheroids with peripheral beads are characterized by high N/C atomic ratios of *ca.* 3–7 × 10^{-2}, which is an order of magnitude higher than those typically determined in bulk Archean kerogens (Watanabe et al., 1997; Beaumont and Robert, 1999; Jia and Kerrich, 2005) and in other spheroid types (Fig. 2). Moreover, they are also slightly enriched in P (Fig. 2).

3.4. Evidence for the biological affinity of film-like microstructures

Film-like microstructures have also been recovered in the SPF acid maceration residue (Fig. 8). Films have been reported from numerous Archean cherts (Westall et al., 2006; Sugitani et al., 2007, 2010). It has been proposed that they formed either from fossilized extracellular polymeric substances (EPS; Westall et al., 2006) secreted by prokaryotic and/or eukaryotic microorganisms, or from condensation of insoluble or soluble OM followed by polymerization into kerogen or pyrobitumen (Sugitani et al., 2010).

Some SPF isolated film-like microstructures present fibrillary 3D networks, exhibiting a striking morphological resemblance with modern EPS (Defarge et al., 1996; Fig. 8a-c, g; see Supplementary Fig. 2 for a zoom onto fibrillary networks). Modern EPS consist in a 3D fibrillar organic network, are mostly composed of polysaccharides, lipopolysaccharides, peptides and glycoproteins (Klock et al., 2007), and are characterized by high N/C atomic ratios of up to 0.16 (Decho et al., 2005). However, in contrast to modern EPS, the film-like microfossils investigated here do not exhibit high N/C atomic ratios (7 × 10^{-3}; Fig. 2), even though early entombment within silica has been proposed to minimize the chemical degradation of microorganisms during advanced diagenesis (Alleon et al., 2016).

Other film-like microstructures present a continuous wall surface (Fig. 8d-f). They are associated with high emissions of $^{12}C^{14}N^-$ yielding N/C atomic ratios reaching values up to 0.13–0.18 (Fig. 2), close to those determined on other films observed on freshly fractured chert surfaces from the same outcrop (0.23–0.25; Alleon et al., 2018) and on modern microbial mats and EPS (Decho et al., 2005). These films also exhibit substantial emissions of $^{31}P^-$ when compared to the polycarbonate filter (Fig. 2). In OM, P may reflect remnants of phospholipids, which are major components of cell membranes, therefore arguing for a high preservation level of the cell membranes. Taken together, all these observations tend to support a biological affinity for film-like microstructures. Although high morphological and geochemical preservation features are associated with films with a continuous wall surface rather than with fibrillary films, this does not imply that fibrillary films constitute the degraded forms of films with continuous walls. Indeed, laboratory experiments have shown that thermal degradation of chemically distinct organic precursors can yield chemically distinct residues (Alleon et al., 2017). It thus seems that the "film-like" morphotype encompasses a morphological and geochemical heterogeneity that cannot yet be assigned to either taphonomic degradation or to distinct organic precursors.

3.5. Occurrence of phosphorus micrometric patches in lenticular fusiform microfossils

Lenses have been reported in several Archean rocks from the Australian and South-African cratons (Walsh, 1992; Sugitani et al., 2007, 2015a, 2018; Oehler et al., 2017). In the studied SPF acid-maceration residue, the "lense" morphotype comprises flanged vesicles (Fig. 9a-b) and non-flanged fusiform carbonaceous microstructures (Fig. 9c-f). Flanged vesicles have been interpreted as possible remnants of autotrophic phytoplanktonic microorganisms owing to their flange-like appendage and their $\delta^{13}C$ signatures (Sugitani et al., 2007, 2015a, 2018; House et al., 2013; Delarue et al., 2017; Oehler et al., 2017; Kozawa et al., 2019). Here, flanged microstructures are presented in Fig. 9a and b and exhibit a hollow central body and a reticulated discoidal flange surrounding this central body as previously described (Sugitani et al., 2015a).

In contrast to these flanged vesicles for which biogenicity is well accepted (Sugitani et al., 2015a, 2018; Oehler et al., 2017; Wacey et al., 2018), the biogenicity of non-flanged fusiform carbonaceous microstructures is still a controversial issue. Wacey et al. (2018), for example, suggested that fusiform carbonaceous microstructures from the 3.48 Gyr-old Dresser Formation could represent silicified vesicular volcanic glasses. As stressed before, studied microstructures are carbonaceous and do not fall within this scope. The carbonaceous fusiform microstructures studied here comprise a 3D coherent and continuous wall surface characterized by high N and P abundances (as suggested by $^{31}P^-/^{12}C_2^-$ ionic ratios) compared to the polycarbonate filter (Figs. 2 and 9).

Phosphorus is essential for life, being both a nutrient and an important component of microbial cells and walls through phospholipid acids and phosphorus-rich granules. Characterizing P abundance and distribution in carbonaceous microstructures may thus provide a powerful criterion to assess their biogenicity. Despite its significance for life biogeochemistry, the occurrence of P in the field of early life remains poorly documented. For instance, Kilburn and Wacey (2008) demonstrated the occurrence of inorganic P in ambient inclusion trails in a sandstone unit of the SPF. In the isolated fusiform lenses, high $^{31}P^-/^{12}C_2^-$ and $^{12}C^{14}N^-/^{12}C_2^-$ ionic ratios are systematically recorded on continuous surfaces, which are less prone to microtopographic artefacts known to bias ion emissions (Thomen et al., 2014; Delarue et al., 2017). Elevated emission of $^{31}P^-$ does not seem to be related to the occurrence of P-rich micron sized minerals either, suggesting that the measured P is bound to OM. NanoSIMS imaging thus suggests, for the first time, that P can be preserved within 3.46 Gyr-old microfossils, indicating a high preservation level of the cell membrane, which is consistent with their good morphological preservation and elevated abundance of N, as also observed in spheroid and film-like microfossils.

In addition to the rather homogeneous distribution of P observed across the surface of well-preserved fusiform microfossils, submicron-sized P patches were also observed in some fusiform lenses (Fig. 9i and l). These P patches are not related to the presence of mineral phases on the microfossil surfaces. These observed P patches may thus correspond either to fossilized polyphosphate granules, used by modern organisms as an energy store (Achbergerova and Nahalka, 2011; Racki et al., 2017), or to P-rich granules formed via sporulation during N starvation (Tocheva et al., 2013), which may have occurred during the Archean eon (Navarro-Gonzalez et al., 2001). Although we cannot disentangle these two possibilities using our current dataset on these SPF microfossils, a possible N starvation would echo recent findings showing that 3.0 Gyr lenses from the Farrel Quartzite in western Australia are characterized by elevated and positive $\delta^{15}N$ values (up to 31‰) interpreted as reflecting a large but partial uptake of NH_4^+ involving Rayleigh fractionation (Delarue et al., 2018b). Nonetheless, we suggest that the $^{31}P^-$ spatial distribution observed on some of the SPF lenses, i.e. those exhibiting higher P/C ionic ratios than polycarbonate filter, can be considered as an unequivocal biological signature, providing here the oldest evidence for cellular organization in the geological record.

4. Conclusion

Four morphological types of microfossils/microstructures, namely filaments, spheroids, films, and lenses, were observed in the acid residue of a sample of the 3.46 Gyr-old Strelley Pool Formation. Most of the microfossils exhibit a discontinuous cell wall related to a poor level of geochemical preservation. However, some spheroids, films and lenses also comprise exceptionally well-preserved specimens characterized by continuous cell-wall surfaces. These well-preserved microfossils are characterized by elevated N and P abundances, highlighting their high level of geochemical preservation.

Although the Strelley Pool microfossils investigated here all underwent a similar diagenetic history involving early silicification, they exhibit a large range of morphological and geochemical preservation levels, encompassing well preserved microfossils (with continuous walls and high N and P contents) and degraded microfossils (with discontinuous walls and low N and P contents). Whether this heterogeneity relates to (i) the expression of a taphonomic gradient having affected differently similar precursor microorganisms, or (ii) the expression of an original biodiversity having produced chemically distinct residues remains an open question.

The Strelley Pool microfossils exhibiting the highest level of morphological and geochemical preservation constitute the best targets to investigate the characteristics of ancient metabolisms and may serve as references for evaluating the biogenicity of other Archean organic microstructures of putative biogenic origin.

Acknowledgments

This research is supported by the ERC Grant No. 290861 – PaleoNanoLife (PI F. Robert; ERC Grant No. 290861). We also thank INSU (Institut National des Sciences de l'Univers) through PNP (Plan National de Planétologie program) and the UK Science and Technology Facilities Council (grant ST/P005225/1 to Romain Tartèse) for financial support. The National NanoSIMS Facility at the MNHN is supported by MNHN, CNRS, Région Ile de France, and Ministère de l'Enseignement Supérieur et de la Recherche. The authors also express their gratitude to V. Rouchon and O. Belhadj (Center for Research on the Preservation of Collections, USR 3224) for Raman spectroscopy. Finally, we are grateful to the two anonymous reviewers for their constructive comments.

Appendix A. Supplementary data

Supplementary data to this article can be found online at https://doi.org/10.1016/j.precamres.2019.105472.

References

Achbergerova, L., Nahalka, J., 2011. Polyphosphate - an ancient energy source and active metabolic regulator. Microb. Cell Fact. 10.
Alleon, J., Bernard, S., Le Guillou, C., Beyssac, O., Sugitani, K., Robert, F., 2018. Chemical nature of the 3.4 Ga Strelley Pool microfossils. Geochem. Perspect. Lett. 7, 37–42.
Alleon, J., Bernard, S., Le Guillou, C., Daval, D., Skouri-Panet, F., Kuga, M., Robert, F., 2017. Organic molecular heterogeneities can withstand diagenesis. Sci. Rep. 7.
Alleon, J., Bernard, S., Le Guillou, C., Daval, D., Skouri-Panet, F., Pont, S., Delbes, L., Robert, F., 2016. Early entombment within silica minimizes the molecular degradation of microorganisms during advanced diagenesis. Chem. Geol. 437, 98–108.
Allwood, A.C., Burch, I.W., Walter, M.R., 2007. Stratigraphy and facies of the 3.43 Ga Strelley Pool Chert in the southwestern part of the North Pole Dome, Pilbara Craton, Western Australia. Geological Survey of Western Australia Record 2007-11.
Allwood, A.C., Kamber, B.S., Walter, M.R., Burch, I.W., Kanik, I., 2010. Trace elements record depositional history of an Early Archean stromatolitic carbonate platform. Chem. Geol. 270, 148–163.
Allwood, A.C., Walter, M.R., Kamber, B.S., Marshall, C.P., Burch, I.W., 2006. Stromatolite reef from the Early Archaean era of Australia. Nature 441, 714–718.
Awramik, S.M., Schopf, J.W., Walter, M.R., 1983. Filamentous fossil bacteria from the Archean of Western Australia. Precambr. Res. 20, 357–374.
Beaumont, V., Robert, F., 1999. Nitrogen isotope ratios of kerogens in Precambrian cherts: a record of the evolution of atmosphere chemistry? Precambr. Res. 96, 63–82.
Bernard, S., Horsfield, B., 2014. Thermal Maturation of Gas Shale Systems. Annu. Rev. Earth Planet. Sci. 42 (42), 635–651.
Buick, R., 1990. Microfossil Recognition in Archean Rocks: an Appraisal of Spheroids and Filaments from a 3500 M.Y. old Chert-Barite Unit at North Pole, Western Australia. Palaios 5, 441–459.
Buick, R., 1984. Carbonaceous filaments from North-Pole, Western Australia – are they fossil bacteria in archean stromatolites. Precambr. Res. 24, 157–172.
Cosmidis, J., Templeton, A.S., 2016. Self-assembly of biomorphic carbon/sulfur microstructures in sulfidic environments. Nat. Commun. 7.
Curiale, J.A., 1986. Origin of solid bitumens, with emphasis on biological marker results. Org. Geochem. 10, 559–580.
Decho, A.W., Visscher, P.T., Reid, R.P., 2005. Production and cycling of natural microbial exopolymers (EPS) within a marine stromatolite. Palaeogeogr. Palaeoclimatol. Palaeoecol. 219, 71–86.
Defarge, C., Trichet, J., Jaunet, A.M., Robert, M., Tribble, J., Sansone, F.J., 1996. Texture of microbial sediments revealed by cryo-scanning electron microscopy. J. Sediment. Res. 66, 935–947.
Delarue, F., Derenne, S., Sugitani, K., Baudin, F., Westall, F., Kremer, B., Tartese, R., Gonzalez, A., Robert, F., 2018a. What is the meaning of hydrogen-to-carbon ratio determined in Archean organic matter? Org. Geochem. 122, 140–146.
Delarue, F., Robert, F., Sugitani, K., Tartese, R., Duhamel, R., Derenne, S., 2017. Investigation of the Geochemical Preservation of ca. 3.0 Ga Permineralized and Encapsulated Microfossils by Nanoscale Secondary Ion Mass Spectrometry. Astrobiology 17, 1192–1202.
Delarue, F., Robert, F., Sugitani, K., Tartese, R., Duhamel, R., Derenne, S., 2018b. Nitrogen isotope signatures of microfossils suggest aerobic metabolism 3.0 Gyr ago. Geochem. Perspect. Lett. 7, 32–36.
Delarue, F., Robert, F., Tartese, R., Sugitani, K., Tang, Q., Duhamel, R., Pont, S., Xiao, S.H., 2018c. Can NanoSIMS probe quantitatively the geochemical composition of ancient organic-walled microfossils? A case study from the early Neoproterozoic Liulaobei Formation. Precambr. Res. 311, 65–73.
Delarue, F., Rouzaud, J.N., Derenne, S., Bourbin, M., Westall, F., Kremer, B., Sugitani, K., Deldicque, D., Robert, F., 2016. The Raman-Derived Carbonization Continuum: A Tool to Select the Best Preserved Molecular Structures in Archean Kerogens. Astrobiology 16, 407–417.
Durand, B. (Ed.), 1980. Kerogen — Insoluble Organic Matter from Sedimentary Rocks. Edition Technip, Paris, pp. 519.
Garcia-Ruiz, J.M., Hyde, S.T., Carnerup, A.M., Christy, A.G., Van Kranendonk, M.J., Welham, N.J., 2003. Self-assembled silica-carbonate structures and detection of ancient microfossils. Science 302, 1194–1197.
Hickman, A.H., 2008. Regional Review of the 3426–3350 Ma Strelley Pool Formation, Pilbara Craton, Western Australia. Geological Survey of Western Australia, Record 2008/15.
House, C.H., Oehler, D.Z., Sugitani, K., Mimura, K., 2013. Carbon isotopic analyses of ca. 3.0 Ga microstructures imply planktonic autotrophs inhabited Earth's early oceans. Geology 41, 651–654.
Jehlicka, J., Beny, C., 1992. Application of Raman microspectrometry in the study of structural-changes in Precambrian kerogens during regional metamorphism. Org. Geochem. 18, 211–213.
Jia, Y., Kerrich, R., 2005. A N-15-enriched Archean atmosphere. Geochimica Et Cosmochimica Acta 69, A395–A395.Kilburn, M.R., Wacey, D., 2008. NanoSIMS analysis of Archean fossils and biomarkers. Appl. Surf. Sci. 255, 1465–1467.
Kiyokawa, S., Ito, T., Ikehara, M., Kitajima, F., 2006. Middle Archean volcano-hydrothermal sequence: Bacterial microfossil-bearing 3.2 Ga Dixon Island Formation, coastal Pilbara terrane, Australia. Geol. Soc. Am. Bull. 118, 3–22.
Kilburn, M.R., Wacey, D., 2008. NanoSIMS analysis of Archean fossils and biomarkers. Appl. Surf. Sci. 255, 1465–1467.
Klock, J.H., Wieland, A., Seifert, R., Michaelis, W., 2007. Extracellular polymeric substances (EPS) from cyanobacterial mats: characterisation and isolation method optimisation. Mar. Biol. 152, 1077–1085.
Kozawa, T., Sugitani, K., Oehler, D.Z., House, C.H., Saito, I., Watanabe, T., Gotoh, T., 2019. Early Archean planktonic mode of life: Implications from fluid dynamics of lenticular microfossils. Geobiology 17, 113–126.
Kremer, B., Kazmierczak, J., 2017. Cellularly preserved microbial fossils from similar to 3.4 Ga deposits of South Africa: A testimony of early appearance of oxygenic life? Precambr. Res. 295, 117–129.
Ledevin, M., Arndt, N., Simionovici, A., Jaillard, E., Ulrich, M., 2014. Silica precipitation triggered by clastic sedimentation in the Archean: New petrographic evidence from cherts of the Kromberg type section, South Africa. Precambr. Res. 255, 316–334.
Lepot, K., Williford, K.H., Ushikubo, T., Sugitani, K., Mimura, K., Spicuzza, M.J., Valley, J.W., 2013. Texture-specific isotopic compositions in 3.4 Gyr old organic matter support selective preservation in cell-like structures. Geochim. Cosmochim. Acta 112, 66–86.
Navarro-Gonzalez, R., McKay, C.P., Mvondo, D.N., 2001. A possible nitrogen crisis for Archaean life due to reduced nitrogen fixation by lightning. Nature 412, 61–64.
Oehler, D.Z., Walsh, M.M., Sugitani, K., Liu, M.C., House, C.H., 2017. Large and robust lenticular microorganisms on the young Earth. Precambr. Res. 296, 112–119.
Oehler, D.Z., Robert, F., Walter, M.R., Sugitani, K., Allwood, A., Meibom, A., Mostefaoui, S., Selo, M., Thomen, A., Gibson, E.K., 2009. NanoSIMS: Insights to biogenicity and syngeneity of Archaean carbonaceous structures. Precambr. Res. 173, 70–78.
Racki, L.R., Tocheva, E.I., Dieterle, M.G., Sullivan, M.C., Jensen, G.J., Newman, D.K., 2017. Polyphosphate granule biogenesis is temporally and functionally tied to cell cycle exit during starvation in Pseudomonas aeruginosa. Proc. Natl. Acad. Sci. U.S.A. 114, E2440–E2449.
Rasmussen, B., 2000. Filamentous microfossils in a 3,235-million-year-old volcanogenic massive sulphide deposit. Nature 405, 676–679.
Rouillard, J., Garcia-Ruiz, J.M., Gong, J., van Zuilen, M.A., 2018. A morphogram for

silica-witherite biomorphs and its application to microfossil identification in the early earth rock record. Geobiology 16, 279–296.
Sanei, H., Wood, J.M., Ardakani, O.H., Clarkson, C.R., Jiang, C.Q., 2015. Characterization of organic matter fractions in an unconventional tight gas siltstone reservoir. Int. J. Coal Geol. 150, 296–305.
Schopf, J.W., Kitajima, K., Spicuzza, M.J., Kudryavtsev, A.B., Valley, J.W., 2018. SIMS analyses of the oldest known assemblage of microfossils document their taxon-correlated carbon isotope compositions. PNAS 115, 53–58.
Sugitani, K., Grey, K., Allwood, A., Nagaoka, T., Mimura, K., Minami, M., Marshall, C.P., Van Kranendonk, M.J., Walter, M.R., 2007. Diverse microstructures from Archaean chert from the mount goldsworthy-mount grant area, pilbara craton, western australia: Microfossils, dubiofossils, or pseudofossils? Precambr. Res. 158, 228–262.
Sugitani, K., Kohama, T., Mimura, K., Takeuchi, M., Senda, R., Morimoto, H., 2018. Speciation of Paleoarchean Life Demonstrated by Analysis of the Morphological Variation of Lenticular Microfossils from the Pilbara Craton, Australia. Astrobiology 18, 1057–1070.
Sugitani, K., Lepot, K., Nagaoka, T., Mimura, K., Van Kranendonk, M., Oehler, D.Z., Walter, M.R., 2010. Biogenicity of Morphologically Diverse Carbonaceous Microstructures from the ca. 3400Ma Strelley Pool Formation, in the Pilbara Craton, Western Australia. Astrobiology 10, 899–920.
Sugitani, K., Mimura, K., Nagaoka, T., Lepot, K., Takeuchi, M., 2013. Microfossil assemblage from the 3400 Ma Strelley Pool Formation in the Pilbara Craton, Western Australia: Results form a new locality. Precambr. Res. 226, 59–74.
Sugitani, K., Mimura, K., Takeuchi, M., Lepot, K., Ito, S., Javaux, E.J., 2015a. Early evolution of large micro-organisms with cytological complexity revealed by micro-analyses of 3.4Ga organic-walled microfossils. Geobiology 13, 507–521.
Sugitani, K., Mimura, K., Takeuchi, M., Yamaguchi, T., Suzuki, K., Senda, R., Asahara, Y., Wallis, S., Van Kranendonk, M.J., 2015b. A Paleoarchean coastal hydrothermal field inhabited by diverse microbial communities: the Strelley Pool Formation, Pilbara Craton, Western Australia. Geobiology 13, 522–545.
Thomen, A., Robert, F., Remusat, L., 2014. Determination of the nitrogen abundance in organic materials by NanoSIMS quantitative imaging. J. Anal. At. Spectrom. 29, 512–519.
Tocheva, E.I., Dekas, A.E., McGlynn, S.E., Morris, D., Orphan, V.J., Jensen, G.J., 2013. Polyphosphate Storage during Sporulation in the Gram-Negative Bacterium Acetonema longum. J. Bacteriol. 195, 3940–3946.
Ueno, Y., Isozaki, Y., Yurimoto, H., Maruyama, S., 2001. Carbon isotopic signatures of individual archean microfossils(?) from Western Australia. Int. Geol. Rev. 43, 196–212.
Wacey, D., Kilburn, M.R., Saunders, M., Cliff, J., Brasier, M.D., 2011. Microfossils of sulphur-metabolizing cells in 3.4-billion-year-old rocks of Western Australia. Nat. Geosci. 4, 698–702.
Wacey, D., Menon, S., Green, L., Gerstmann, D., Kong, C., McLoughlin, N., Saunders, M., Brasier, M., 2012. Taphonomy of very ancient microfossils from the similar to 3400 Ma Strelley Pool Formation and similar to 1900 Ma Gunflint Formation: New insights using a focused ion beam. Precambr. Res. 220, 234–250.
Wacey, D., Noffke, N., Saunders, M., Guagliardo, P., Pyle, D.M., 2018. Volcanogenic Pseudo-Fossils from the similar to 3.48 Ga Dresser Formation, Pilbara, Western Australia. Astrobiology 18, 539–555.
Walsh, M.M., 1992. Microfossils and possible microfossils from the early archean onverwacht group, Barberton mountain land, South-Africa. Precambr. Res. 54, 271–293.
Walsh, M.M., Lowe, D.R., 1985. Filamentous microfossils from the 3,500-myr-old Onverwacht Group, Barberton Mountain Land, South-Africa. Nature 314, 530–532.
Van Kranendonk, M.J., 1999. North Shaw W.A. Sheet 2755: 1:100 000 Geological Series. Western Australia Geological Survey.
Watanabe, K., Naraoka, H., Wronkiewicz, D.J., Condie, K.C., Ohmoto, H., 1997. Carbon, nitrogen, and sulfur geochemistry of Archean and Proterozoic shales from the Kaapvaal Craton, South Africa. Geochim. Cosmochim. Acta 61, 3441–3459.
Westall, F., de Ronde, C.E.J., Southam, G., Grassineau, N., Colas, M., Cockell, C., Lammer, H., 2006. Implications of a 3.472-3.333-Gyr-old subaerial microbial mat from the Barberton greenstone belt, South Africa for the UV environmental conditions on the early Earth. Philos. Trans. R. Soc. B 361, 1857–1875.
Westall, F., de Wit, M.J., Dann, J., van der Gaast, S., de Ronde, C.E.J., Gerneke, D., 2001. Early Archean fossil bacteria and biofilms in hydrothermally-influenced sediments from the Barberton greenstone belt, South Africa. Precambr. Res. 106, 93–116.